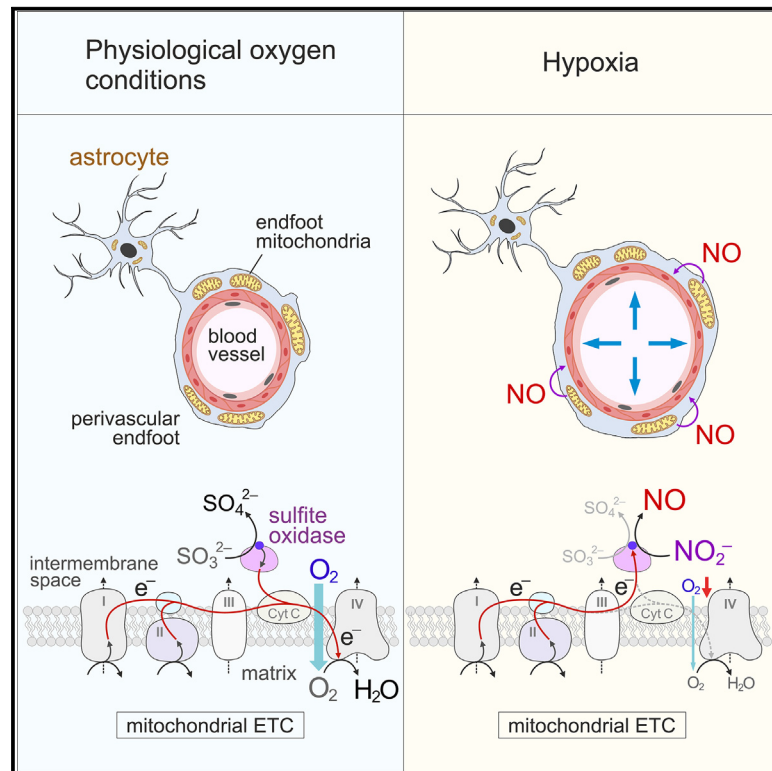


Astrocytes produce nitric oxide via nitrite reduction in mitochondria to regulate cerebral blood flow during brain hypoxia

Graphical abstract



Authors

Isabel N. Christie,
Shefeeq M. Theparambil, Alice Braga, ...,
Andrey Y. Abramov,
Plamena R. Angelova,
Alexander V. Gourine

Correspondence

s.theparambil@ucl.ac.uk (S.M.T.),
a.gourine@ucl.ac.uk (A.V.G.)

In brief

How does the brain maintain its oxygen supply during hypoxia? Christie, Theparambil et al. show that in response to hypoxia, brain astrocytes produce nitric oxide (NO) via nitrite reduction in mitochondria. They identify astrocyte mitochondria as brain oxygen sensors that regulate cerebral blood flow through release of the potent vasodilator NO.

Highlights

- Brain astrocytes produce nitric oxide (NO) in response to hypoxia
- During hypoxia, NO is generated via nitrite reduction in astrocyte mitochondria
- NO is produced by the molybdenum-containing mitochondrial enzyme sulfite oxidase
- This astroglial mechanism mediates increases in cerebral blood flow during hypoxia



Article

Astrocytes produce nitric oxide via nitrite reduction in mitochondria to regulate cerebral blood flow during brain hypoxia

Isabel N. Christie,^{1,9} Shefeeq M. Theparambil,^{1,9,*} Alice Braga,¹ Maxim Doronin,² Patrick S. Hosford,¹ Alexey Brazhe,^{3,4} Alexander Mascarenhas,¹ Shereen Nizari,^{1,5} Anna Hadjihambi,⁶ Jack A. Wells,⁵ Adrian Hobbs,⁷ Alexey Semyanov,^{2,3} Andrey Y. Abramov,⁸ Plamena R. Angelova,⁸ and Alexander V. Gourine^{1,10,*}

¹Centre for Cardiovascular and Metabolic Neuroscience, Department of Neuroscience, Physiology & Pharmacology, University College London, London WC1E 6BT, UK

²College of Medicine, Jiaxing University, Jiaxing 314001, China

³Department of Molecular Neurobiology, Institute of Bioorganic Chemistry, Moscow 117997, Russian Federation

⁴Faculty of Biology, Lomonosov Moscow State University, Moscow 119234, Russian Federation

⁵Centre for Advanced Biomedical Imaging, Division of Medicine, University College London, London WC1E 6BT, UK

⁶The Roger Williams Institute of Hepatology, Foundation for Liver Research, and Faculty of Life Sciences and Medicine, King's College London, London SE5 9NT, UK

⁷William Harvey Research Institute, Barts and The London School of Medicine, Queen Mary University of London, London EC1M 6BQ, UK

⁸Department of Clinical and Movement Neurosciences, Queen Square Institute of Neurology, University College London, London WC1N 3BG, UK

⁹These authors contributed equally

¹⁰Lead contact

*Correspondence: s.theparambil@ucl.ac.uk (S.M.T.), a.gourine@ucl.ac.uk (A.V.G.)

<https://doi.org/10.1016/j.celrep.2023.113514>

SUMMARY

During hypoxia, increases in cerebral blood flow maintain brain oxygen delivery. Here, we describe a mechanism of brain oxygen sensing that mediates the dilation of intraparenchymal cerebral blood vessels in response to reductions in oxygen supply. *In vitro* and *in vivo* experiments conducted in rodent models show that during hypoxia, cortical astrocytes produce the potent vasodilator nitric oxide (NO) via nitrite reduction in mitochondria. Inhibition of mitochondrial respiration mimics, but also occludes, the effect of hypoxia on NO production in astrocytes. Astrocytes display high expression of the molybdenum-cofactor-containing mitochondrial enzyme sulfite oxidase, which can catalyze nitrite reduction in hypoxia. Replacement of molybdenum with tungsten or knockdown of sulfite oxidase expression in astrocytes blocks hypoxia-induced NO production by these glial cells and reduces the cerebrovascular response to hypoxia. These data identify astrocyte mitochondria as brain oxygen sensors that regulate cerebral blood flow during hypoxia via release of nitric oxide.

INTRODUCTION

The brain is extremely vulnerable to reductions in oxygen supply (hypoxia) due to its exceptionally high metabolic rate associated with the activities of billions of neurons.¹ If brain blood supply were suddenly to cease, the cerebral oxygen content (~0.03 mM) would be enough to maintain neuronal function for only a few seconds.^{2,3} Specialized peripheral (arterial) oxygen sensors are located outside the CNS (in the carotid and aortic bodies) and cannot directly detect brain tissue hypoxia, let alone regional differences in brain tissue oxygenation.⁴ This points to the necessity and importance of intrinsic brain mechanisms of oxygen sensing that can induce dilation of brain blood vessels and increase cerebral blood flow in response to hypoxia.

The cerebral vasculature is indeed sensitive to arterial hypoxemia and/or brain tissue hypoxia.^{5,6} Studies of the mechanisms

underlying hypoxia-induced responses of cerebral blood vessels highlighted the potential roles of ATP-sensitive K⁺ channels, as well as signaling mediated by protons, lactate, ATP, adenosine, and nitric oxide (NO).^{5,6} However, the exact mechanisms of hypoxic cerebral vasodilation are not fully understood and there are controversies surrounding the involvement of previously proposed signaling pathways. Understanding regulation of cerebral blood flow in hypoxia is important, as there are significant gradients in brain tissue partial pressure of oxygen (PO₂) even at normal arterial PO₂ and saturation,^{7,8} suggesting that some brain regions may experience critical reductions of oxygen supply.^{9,10} The risk of brain hypoxia increases with aging and under specific conditions such as exposure to high altitude, lung disease, or sleep apnea.

All penetrating and intraparenchymal cerebral blood vessels are wrapped by the endfeet of astrocytes—omnipresent multifunctional glial cells that control the cerebral vasculature via



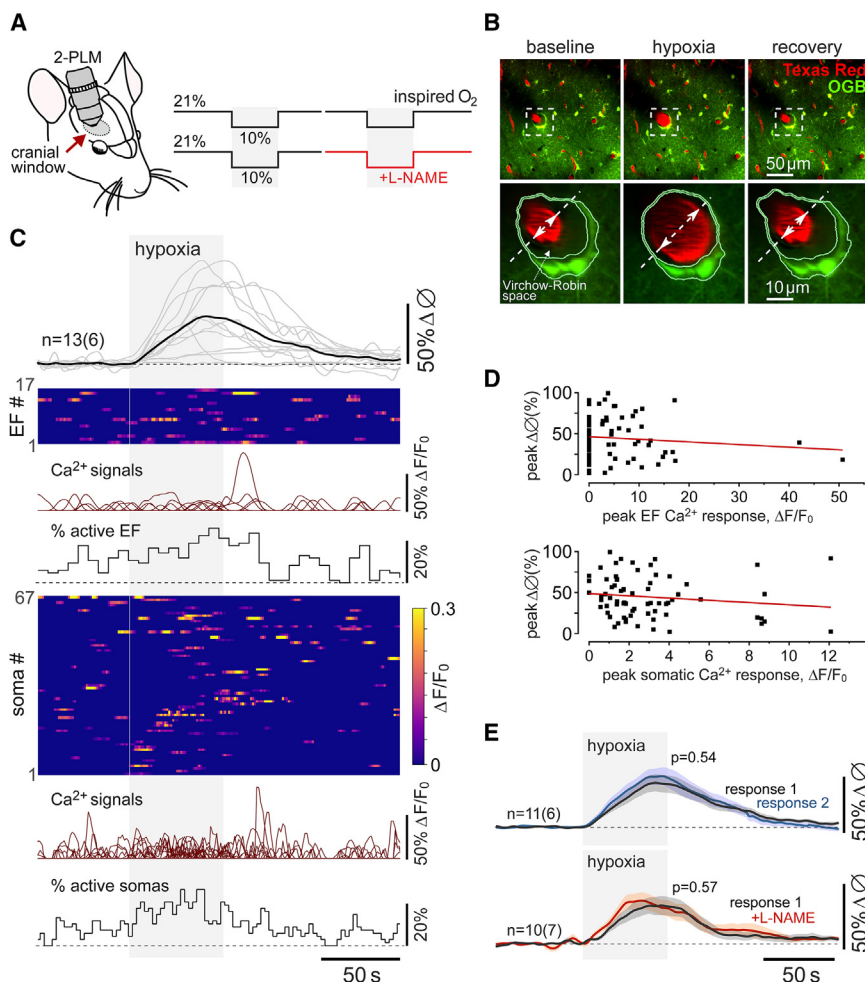


Figure 1. Hypoxia-induced vascular responses in the cerebral cortex

(A) Diagram of the experimental protocol in anesthetized rats instrumented for two-photon imaging of cortical blood vessels (visualized with intravascular dye Texas Red) and Ca^{2+} in cortical astrocytes (using the Ca^{2+} -sensitive dye Oregon Green BAPTA 1 AM [OGB]). 2-PLM, two-photon laser scanning microscopy.

(B) Representative images taken near the cortical surface at baseline, at the peak of the response induced by 10% inspired O_2 , and after a complete recovery from hypoxia, illustrating changes in the vessel diameter and segmentation of the astrocyte endfoot.

(C) Hypoxia-induced changes in the diameter of penetrating cortical arterioles (13 vessels recorded in 6 animals), Ca^{2+} signals in perivascular endfeet (EF; 17 regions of interest [ROIs]) and cell bodies (67 ROIs) of cortical astrocytes. Ca^{2+} responses in the astrocyte endfeet and cell bodies are illustrated as raster plots, overlays of individual Ca^{2+} traces, and time-binned percentages of active ROIs.

(D) Scatterplots showing the relations between the hypoxia-induced Ca^{2+} responses in astrocyte endfeet and cell bodies and the corresponding cerebrovascular dilations.

(E) Summary data showing overlaid profiles of changes in the diameter of penetrating cortical arterioles in response to two sequential episodes of hypoxia (10% inspired O_2). Hypoxia triggered reproducible dilations of cortical vessels that were not affected in conditions of established systemic nitric oxide synthase (NOS) blockade with N(ω)-nitro-L-arginine methyl ester (L-NAME; 10 mg kg^{-1}). The data are shown as means \pm SEM. n = number of vessels (number of animals). p values, Wald test on linear mixed-effect model with random intercepts.

Ca^{2+} -dependent release of vasoactive signaling molecules.^{11,12} In this study, we tested the hypothesis that astrocytes are brain oxygen sensors that induce dilation of intraparenchymal cerebral blood vessels and increase brain tissue perfusion in response to hypoxia.

RESULTS

We first investigated whether hypoxia-induced Ca^{2+} responses in astrocytes¹³ might be responsible for the dilations of cerebral arterioles associated with these glial cells. Using two-photon imaging in anesthetized and artificially ventilated rats, we recorded robust dilations of cortical arterioles (on average by $36\% \pm 3\%$; 65 vessels recorded in 23 animals) when the concentration of inspired oxygen was lowered to 10% (Figures 1A–1C). Reproducible dilations of cortical vessels occurred immediately after the onset of the hypoxic stimulus (Figures 1B and 1C). Cortical astrocytes loaded with the Ca^{2+} -sensitive dye Oregon Green BAPTA 1 AM responded to systemic hypoxia with increased frequency of Ca^{2+} signals in perivascular endfeet and cell bodies (Figures 1C and S1). It was found that 60% of perivascular endfeet and 55% of astrocyte cell bodies responded to hypoxia with elevations in cytosolic $[\text{Ca}^{2+}]$. However, there were no cor-

relations between the vessel dilations and Ca^{2+} responses in astrocyte cell bodies and endfeet (Figure 1D), suggesting that Ca^{2+} -dependent release of vasoactive signaling molecules by astrocytes is unlikely to mediate the cerebrovascular response to hypoxia.

There is evidence that hypoxia-induced increases in cerebral blood flow are mediated by NO.^{6,14} We found that in our experimental conditions, hypoxia-induced dilations of cortical arterioles in response to 10% inspired O_2 were unaffected by systemic NO synthase (NOS) blockade with N(ω)-nitro-L-arginine methyl ester (L-NAME) (Figures 1E and S2), which is consistent with the results of some human¹⁵ and experimental animal studies.¹⁶ However, blockade of cGMP signaling was reported to inhibit the cerebrovascular response to hypoxia,¹⁷ and NO can also be produced by reduction of the nitrite anion (NO_2^-), an alternative mechanism of NO generation by some heme- or molybdenum-cofactor-containing metalloproteins that can transfer an electron and facilitate proton donation.^{18–20}

Astrocytes have a loosely assembled mitochondrial respiratory chain, resulting in less efficient mitochondrial respiration, and a propensity to electron leak.²¹ We next tested the hypothesis that in hypoxia, the electrons from the electron transport chain in astrocyte mitochondria can be used to generate NO via

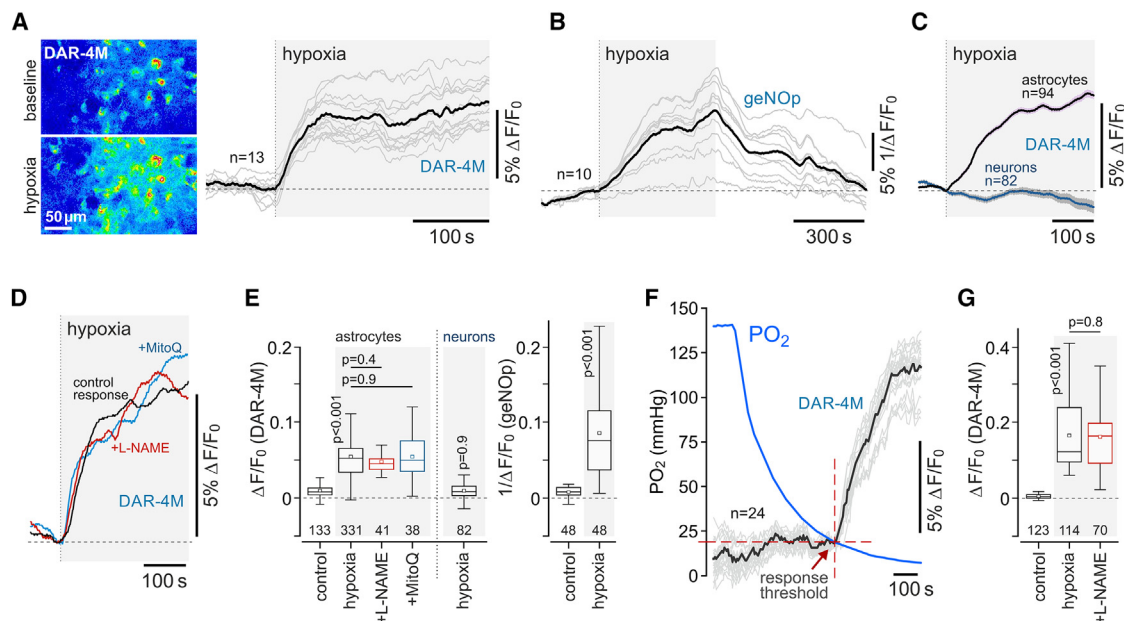


Figure 2. Astrocytes produce NO in response to hypoxia

(A) Hypoxia-induced changes in fluorescence of the NO-sensitive dye DAR-4M in cultured astrocytes. Representative images were taken at baseline and at the peak of the response to hypoxia, induced by the displacement of oxygen by argon. Traces illustrate representative examples of individual (gray) and averaged (black) changes in DAR-4M fluorescence recorded in 13 astrocytes in one experiment.

(B) Hypoxia-induced changes in fluorescence of the genetically encoded NO sensor geNOP, expressed in cultured astrocytes. Traces depict individual (gray) and averaged (black) changes in geNOP fluorescence recorded in 10 astrocytes in one experiment.

(C) Averaged profiles of hypoxia-induced changes in NO production recorded in cortical astrocytes and cerebellar granule neurons.

(D) Hypoxia-induced NO production in astrocytes in the absence and presence of NOS inhibitor L-NAME (100 μ M) or reactive oxygen species scavenger MitoQ (500 μ M). Each trace illustrates averaged changes in DAR-4M fluorescence recorded in 8–15 individual astrocytes in separate experiments.

(E) Summary data illustrating peak changes in DAR-4M and geNOP fluorescence (reporting NO production) recorded in cortical astrocytes in response to hypoxia, also showing the effects of L-NAME and MitoQ on astrocyte responses, and peak hypoxia-induced neuronal responses.

(F) Representative example of data obtained in the experiments in organotypic slices of the cerebral cortex involving simultaneous recordings of NO production by astrocytes and partial pressure of oxygen (PO_2) near the surface of the slice, illustrating the PO_2 threshold of the astrocyte response to hypoxia.

(G) Summary data illustrating peak hypoxia-induced changes in DAR-4M fluorescence recorded in organotypic cortical slices in the absence and presence of L-NAME. In the box-and-whisker plots, numbers above the horizontal line indicate the numbers of individual astrocytes recorded in 4–8 separate cultures prepared from 3–6 animals. In the box-and-whisker plots, the central dot indicates the mean, the central line indicates the median, the box limits indicate the upper and lower quartiles, and the whiskers show the minimum–maximum range of the data. p values, ANOVA.

reduction of NO_2^- . We used the fluorescent NO indicator DAR-4M²² and the genetically encoded NO sensor geNOP²³ to record NO production in cultured astrocytes and neurons (Figure 2). Both indicators reported robust increases in NO production in astrocytes in response to hypoxia induced following displacement of oxygen in the incubation medium by argon (Figures 2A–2C and 2E). Hypoxia-induced NO production in astrocytes was unaffected by NOS inhibitor L-NAME (100 μ M) (Figures 2D, 2E, and 2G) or in the presence of a mitochondrial antioxidant, MitoQ (500 μ M), which scavenges reactive oxygen species, but not NO (Figures 2D and 2E). Hypoxia had no effect on NO production in cerebellar neurons (known to express high levels of neuronal NOS) (Figures 2C and 2E). Experiments conducted in organotypic cortical slices, involving monitoring of PO_2 in the medium, showed that astrocytes begin to produce NO when PO_2 falls below the threshold of 17 ± 2 mmHg (as recorded near the surface of the slice) (Figure 2F).

It was next found that the effect of hypoxia on NO production in astrocytes could be mimicked by chemical inhibition of the

mitochondrial electron transport chain (chemical hypoxia) (Figure 3A). Inhibition of mitochondrial complex I with rotenone (2 μ M), inhibition of complex III with myxothiazol (3 μ M), inhibition of complex IV with cyanide (KCN, 100 μ M) or azide (0.5 mM), or mitochondrial uncoupling with FCCP (1 μ M) triggered robust NO generation by astrocytes and occluded the effect of hypoxia on NO production in these cells (Figures 3B–3D). Blockade of ATP synthase with oligomycin (2 μ M) had no effect on NO production by astrocytes (Figures 3B and 3D). Astrocyte NO production induced by chemical hypoxia (cyanide, myxothiazol) was unaffected by L-NAME (Figures S3A and S3B). Inhibition of mitochondrial respiration with rotenone (2 μ M) or cyanide (100 μ M) had no effect on NO production in cerebellar or cortical neurons (Figure S4).

Mitochondrial inhibition with rotenone was previously reported to selectively occlude the hypoxia-induced responses of the prototypical mammalian oxygen sensors—carotid body glomus cells.^{24,25} We next applied rotenone by microinjection in the vicinity of the imaged arterioles *in vivo*. Rotenone had no effect

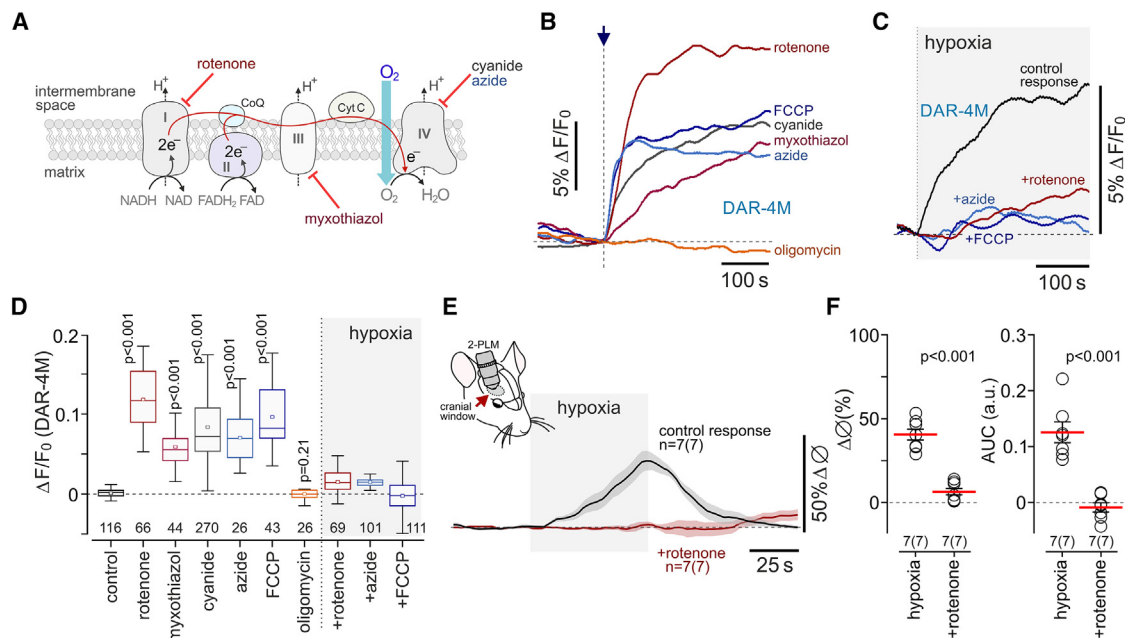


Figure 3. Inhibition of mitochondrial respiration induces NO production in astrocytes and occludes the responses to hypoxia

(A) Schematic drawing of the mitochondrial electron transport chain (ETC) illustrating the sites of action of the inhibitors used in this study. (B) Inhibition of the mitochondrial ETC or mitochondrial uncoupling (rotenone, 2 μ M; myxothiazol, 3 μ M; KCN, 100 μ M; azide, 0.5 mM; FCCP, 1 μ M) triggers NO production in astrocytes. Inhibition of mitochondrial ATP synthase with oligomycin (2 μ M) had no effect. (C) Inhibition of the mitochondrial ETC (rotenone, azide) or mitochondrial uncoupling (FCCP) occlude the effect of hypoxia on NO production in astrocytes. In (B) and (C), each trace shows averaged changes in DAR-4M fluorescence recorded in 10–15 individual astrocytes in separate experiments. (D) Summary data illustrating peak changes in DAR-4M fluorescence recorded in cortical astrocytes in response to inhibition of the mitochondrial ETC or mitochondrial uncoupling and in response to hypoxia in conditions of ETC inhibition or mitochondrial uncoupling. Numbers above the horizontal line indicate the numbers of individual astrocytes recorded in 4–8 separate cultures prepared from 3–6 animals. In the box-and-whisker plots, the central dot indicates the mean, the central line indicates the median, the box limits indicate the upper and lower quartiles, and the whiskers show the minimum–maximum range of the data. p values, ANOVA. (E) Hypoxia-induced dilations of cortical arterioles are blocked by rotenone applied by microinjection in the vicinity of the recorded vessels (anesthetized mice). (F) Summary data illustrating peak and integral (area under the curve [AUC]) hypoxia-induced changes in cortical arteriole diameter following intraparenchymal microinjections of a vehicle (14% DMSO in aCSF) or rotenone (1 mM; 1.5 μ L). The data are shown as individual values and means \pm SEM. n = number of vessels (number of animals). p values, unpaired t test.

on resting vessel diameter (8.2 ± 1.1 vs. 7.9 ± 0.8 μ m in control conditions; n = 7 in each group; p = 0.80) but completely blocked the dilations of cortical arterioles induced by hypoxia (Figures 3E and 3F).

Measurements of $[\text{NO}_2^-]$ in astrocytes or isolated astrocyte mitochondria following incubation of cells with NO_2^- (0, 5, 10, 30, and 100 μ M) showed that in aerobic conditions, astrocyte mitochondria accumulate NO_2^- (Figure 4A). Under resting conditions, the intracellular concentration of NO_2^- in astrocytes was measured at 0.28 ± 0.04 μ M, and the concentration of NO_2^- in astrocyte mitochondria was measured at 1.3 ± 0.2 μ M. $[\text{NO}_2^-]$ increased exponentially with a rising concentration of NO_2^- in the medium, reaching 8.8 ± 0.9 μ M (p = 0.020) in astrocytes (intracellular) and 52.8 ± 3.2 μ M (p = 0.004) in astrocyte mitochondria in conditions of 100 μ M extracellular NO_2^- (Figure 4A). In the presence of supplemental NO_2^- (100 μ M) (but not nitrate, NO_3^-), NO production by astrocytes in response to hypoxic or chemical hypoxia (cyanide) was greatly enhanced (Figures 4B and 4C). This effect of nitrite was blocked by inhibition of anion transport with 4,4'-diisothiocyano-2,2'-stilbenedisulfonic acid (100 μ M) (Figure S3C), point-

ing to the existence of mechanism(s) that transport nitrite across cellular membranes.

Several metalloproteins can facilitate generation of NO by transferring electrons for nitrite reduction.^{18,19} To identify the astroglial mechanism responsible for nitrite reduction in hypoxic conditions, we analyzed RNA sequencing (RNA-seq) data to evaluate the expression of heme-containing and molybdenum (Mo)-bound molybdopterin cofactor-containing enzymes and related proteins in cultured astrocytes, as well as in astrocytes acutely isolated from the cerebral cortex of neonatal (P3) and adult rats (Figure 4D). High relative expression of genes encoding molybdenum cofactor-containing mitochondrial enzyme sulfite oxidase (*Suox* gene) and molybdenum cofactor synthesis protein (*Mocs2* gene; involved in the synthesis of molybdopterin cofactor, required for biochemical activation of molybdenum) was detected in cultured and acutely isolated cortical astrocytes (Figure 4D). High expression of *Suox* and *Mocs2* in cortical astrocytes was confirmed by analysis of data from a publicly available mouse brain transcriptome database²⁶ (Figure S5).

If tungstate is added to the medium, then tungsten effectively replaces molybdenum in molybdopterin-cofactor-containing

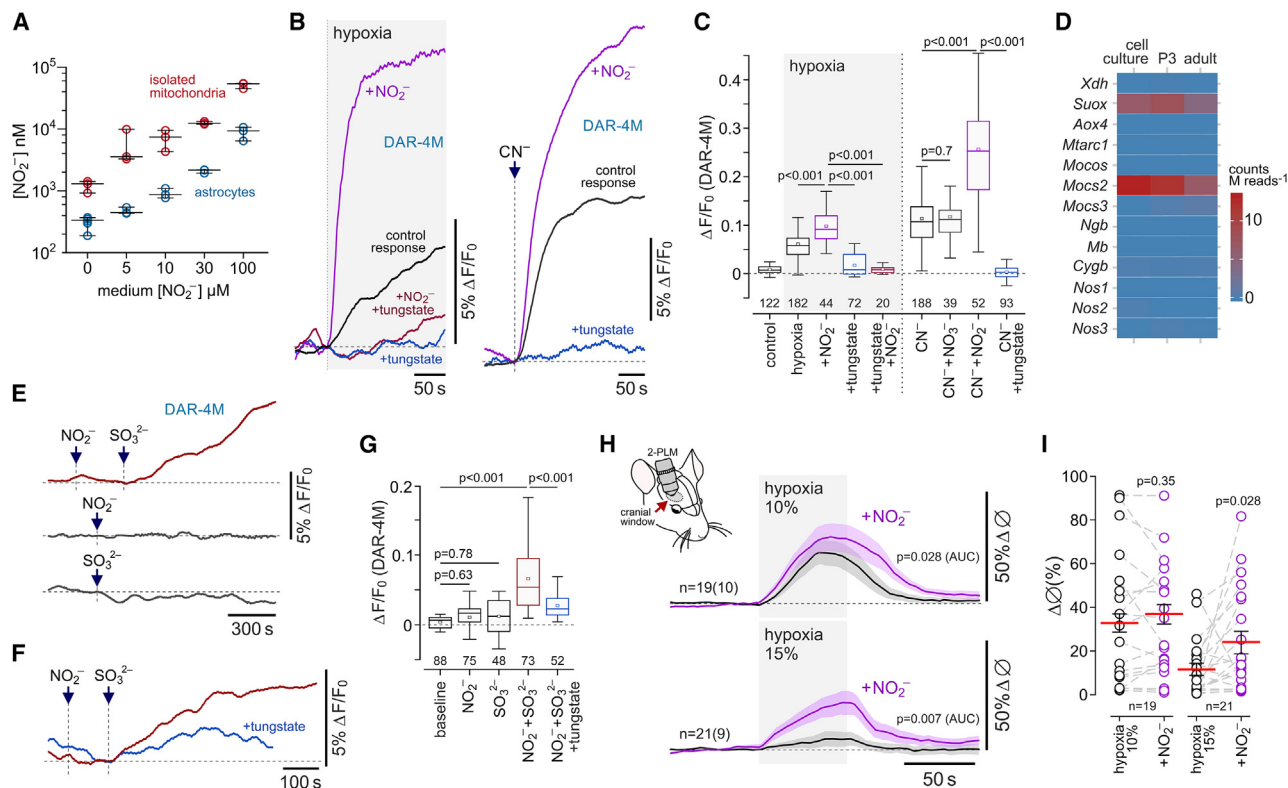


Figure 4. During hypoxia, astrocytes produce NO via nitrite reduction

(A) Astrocyte mitochondria accumulate nitrite. Summary data illustrating measurements of nitrite concentration ($[NO_2^-]$) in astrocytes and isolated astrocyte mitochondria that were incubated for 1 h with $NaNO_2$ (0, 5, 10, 30, 100 μ M) in aerobic conditions.

(B) Astrocyte NO production induced by hypoxia or inhibition of complex IV with cyanide (100 μ M) is augmented by supplemental NO_2^- (100 μ M) and is abolished in cells incubated with tungstate (0.5 mM), which replaces molybdenum with tungsten in molybdopterin cofactor-containing enzymes.

(C) Summary data illustrating peak changes in DAR-4M fluorescence recorded in cortical astrocytes in response to hypoxia or mitochondrial inhibition with cyanide in the absence or presence of supplemental NO_2^- or nitrate (NO_3^-) and after incubation of cells with tungstate. In the box-and-whisker plots, the central dot indicates the mean, the central line indicates the median, the box limits indicate the upper and lower quartiles, and the whiskers show the minimum–maximum range of the data. p values, ANOVA.

(D) RNA-seq data illustrating the expression of genes encoding metalloproteins with nitrite reductase activity and other relevant proteins in cultured cortical astrocytes and acutely isolated cortical astrocytes of neonatal (postnatal day 3) and young adult rats. *Xdh*, xanthine dehydrogenase/oxidase; *Suox*, sulfite oxidase; *Aox4*, aldehyde oxidase 4; *Mtarc1*, mitochondrial amidoxime reducing component; *Mocos*, molybdenum cofactor sulfurylase; *Mocs2* and *-3*, molybdenum cofactor synthesis genes; *Ngb*, neuroglobin; *Mb*, myoglobin; *Cygb*, cytoglobin; *Nos1*, neuronal NOS; *Nos2*, inducible NOS; *Nos3*, endothelial NOS.

(E and F) Sulfite (SO_3^{2-} ; 0.5 mM) induces NO production in astrocytes in the presence of NO_2^- (100 μ M).

(G) Summary data illustrating peak changes in DAR-4M fluorescence recorded in cortical astrocytes in response to NO_2^- , SO_3^{2-} , SO_3^{2-} in the presence of NO_2^- and in response to SO_3^{2-} in the presence of NO_2^- in cells incubated with tungstate. p values, Kruskal-Wallis ANOVA.

In (C) and (G), numbers above the horizontal line indicate the numbers of individual astrocytes recorded in 4–8 separate cultures prepared from 3–6 animals.

(H) Hypoxia-induced arteriole dilations in the cerebral cortex are augmented following systemic treatment with $NaNO_2$ (1 mg kg⁻¹, intravenous). Shown are overlaid profiles of changes in the diameter of penetrating cortical arterioles in response to two sequential episodes of hypoxia (10% or 15% inspired O_2) before and after the administration of nitrite.

(I) Summary data illustrating peak hypoxia-induced increases in cortical arteriole diameter in control conditions and after nitrite administration. The data are shown as individual values and means \pm SEM. p values, Wald test on linear mixed-effect model with random intercepts.

enzymes.²⁷ We found that after 24 h incubation with sodium tungstate (0.5 mM), cultured astrocytes were no longer able to generate NO in response to hypoxic or chemical hypoxia (Figures 4B and 4C), indicating that a molybdopterin cofactor enzyme is responsible for nitrite reduction in these conditions. Xanthine oxidase and aldehyde oxidase (both cytosolic proteins) did not appear to be involved, as potent inhibitors of these enzymes, allopurinol (50 μ M) and oxypurinol (20 μ M),¹⁸ had no effect on hypoxia-induced NO production by astrocytes (Figure S3D).

Sulfite oxidase (which is highly expressed in cortical astrocytes; Figure 4D) catalyzes the oxidation of sulfite (SO_3^{2-}) in the intermembrane space of mitochondria.²⁸ We next hypothesized that if sulfite oxidase is responsible for nitrite reduction in astrocytes, then substrate (sulfite) supplementation should trigger NO production in these cells. Indeed, in the presence of 100 μ M NO_2^- , the addition of sulfite (SO_3^{2-} ; 0.5 mM) evoked NO production by astrocytes in aerobic conditions (Figures 4E and 4G). Neither NO_2^- (100 μ M) nor SO_3^{2-} (0.5 mM) facilitated NO production

when applied individually (Figures 4E and 4G). NO production induced by SO_3^{2-} in the presence of NO_2^- was reduced in astrocytes that were incubated with tungstate (Figures 4F and 4G). These data suggested that sulfite oxidase can effectively transfer electrons for nitrite reduction in astrocyte mitochondria.

If the identified mechanism of NO production contributes to hypoxia-induced increases in cerebrovascular flow, then supplemental NO_2^- would be expected to augment the dilations of cerebral vasculature in response to decreases in inspired O_2 . Systemic administration of nitrite (1 mg kg^{-1}) had no effect on the peak amplitude of cortical arteriole dilations induced by 10% inspired O_2 but increased the overall response (0.12 ± 0.003 vs. 0.11 ± 0.002 area under the curve [AUC] in control conditions; 19 vessels recorded in 10 animals; $p = 0.028$; Figures 4H and 4I). This effect of nitrite was relatively small and could potentially be explained by 10% inspired O_2 causing near-maximal arteriole dilations and exhaustion of the cerebrovascular reserve. Therefore, we next determined the effect of supplemental NO_2^- on cerebrovascular response to moderate hypoxia (Figures 4H and 4I). Peak dilations of cortical arterioles induced by 15% inspired O_2 were increased by 100% following systemic administration of NO_2^- (diameter increase by $24\% \pm 5\%$ vs. $12\% \pm 3\%$ in control conditions; 21 vessels recorded in 9 animals; $p = 0.028$; Figures 4H and 4I). Nitrite administration had no effect on Ca^{2+} responses in astrocyte cell bodies and perivascular endfeet induced by 10% or 15% inspired O_2 (Figure S1B).

To test the hypothesis that sulfite oxidase is responsible for hypoxia-induced NO production by astrocytes and dilation of cerebral blood vessels, we next used viral vectors to express short hairpin RNA (SUOX-shRNA) in order to knock down the expression of this enzyme in cultured astrocytes and *in vivo*. It was found that SUOX-shRNA reduced the expression of sulfite oxidase in astrocytes by 90% (Figure 5A) and blocked the astrocyte NO production induced by hypoxia or mitochondrial inhibition with rotenone or cyanide (Figures 5B and 5C). Intracerebroventricular injections of the AAV5-U6-SUOX-shRNA-EGFP vector in neonatal mice established a patchy expression of the transgene in cortical astrocytes of 3- to 4-month-old mice (Figure 5D). SUOX-shRNA expression in the cortex had no effect on resting vessel diameter ($7.3 \pm 0.7 \mu\text{m}$, $n = 6$ vs. $7.9 \pm 0.7 \mu\text{m}$ in controls, $n = 8$; $p = 0.58$) or the peak dilations of cortical arterioles but reduced the overall vasodilatory responses induced by 10% inspired O_2 by 51% (0.077 ± 0.002 vs. 0.0383 ± 0.001 AUC in controls; $p = 0.043$; Figures 5E and 5F).

DISCUSSION

The data obtained in this study suggest that astrocytes respond to hypoxia by producing NO via nitrite reduction in mitochondria to dilate intraparenchymal cerebral blood vessels and increase brain tissue perfusion. The fact that the effect of chemical inhibition of mitochondrial respiration mimics, but also occludes, the effect of hypoxia points to mitochondria as the site of NOS-independent NO production in astrocytes. Blockade of NO production by tungstate indicates that a molybdopterin cofactor-containing enzyme is responsible for hypoxia-induced nitrite reduction in astrocytes. Mammals express

four members of this family of metalloproteins,^{18,19} and our transcriptome analysis revealed high relative expression of sulfite oxidase in cortical astrocytes. In aerobic conditions and in the presence of supplemental nitrite, astrocytes generated NO in response to sulfite. Knockdown of sulfite oxidase expression in astrocytes prevented the effect of hypoxia on NO production in these cells and reduced the cerebrovascular response to systemic hypoxia. Collectively, these lines of evidence suggest that during hypoxia, sulfite oxidase is responsible for NO production in astrocyte mitochondria (Figure 5G).

In contrast to NO synthesis by enzymes of the NOS family, the generation of NO via nitrite reduction does not require molecular oxygen. This would be particularly advantageous in conditions of reduced oxygen supply and/or increased oxygen demand when rapid NO release and signaling can effectively increase brain tissue perfusion. Low pH favors nitrite reduction by metalloproteins, which transfer an electron and facilitate proton donation.^{18,19} Sulfite oxidase is structurally similar to plant nitrate reductase²⁹ and is located in proximity to cytochrome c within the mitochondrial intermembrane space,³⁰ where conditions for nitrite reduction appear to be ideal (Figure 5G), especially in astrocytes, as these cells have a loosely assembled mitochondrial respiratory chain and a propensity for electron leak.²¹ We hypothesize that electrons for nitrite reduction by sulfite oxidase are derived from complex III (Figure 5G).

There is evidence of significant gradients in brain tissue oxygen concentration, even at normal arterial PO_2 and saturation,^{7,8} suggesting that some brain regions may experience critical reductions of oxygen supply.^{9,10} Our data point to an important physiological role of mitochondria, densely packed in the astroglial perivascular endfeet,³¹ which cover all penetrating and intraparenchymal cerebral blood vessels (Figure 5G). The data suggest that astrocyte mitochondria function as both the physiological sensors of brain tissue oxygen and effectors that can rapidly dilate the associated cerebral blood vessels via release of NO. We hypothesize that this mechanism of NO production by astrocyte mitochondria dynamically matches regional cerebral perfusion to brain tissue oxygen demand and contributes to the increases in global brain blood flow during systemic hypoxia.

Limitations of the study

This study contributes to our understanding of the mechanisms underlying oxygen sensing in the brain. The data show that in response to hypoxia, the mitochondrial enzyme sulfite oxidase generates NO via reduction of nitrite. The lack of pharmacological tools to manipulate sulfite oxidase activity limited our ability to analyze its function in detail. The use of viral vectors to drive the expression of sulfite oxidase shRNA in astrocytes was highly effective in knocking down the expression of the enzyme (by 90%), but shRNA took several days to achieve an effect, which was also irreversible. In this study, we used both female and male animals without differentiation. Although we did not notice any obvious differences in the responses and the effects of experimental treatments between individual replicates, the lack of formal analysis of sex-related differences in the described mechanism is a limitation of the study. Another limitation is the use of anesthesia in the *in vivo* experiments, and future studies

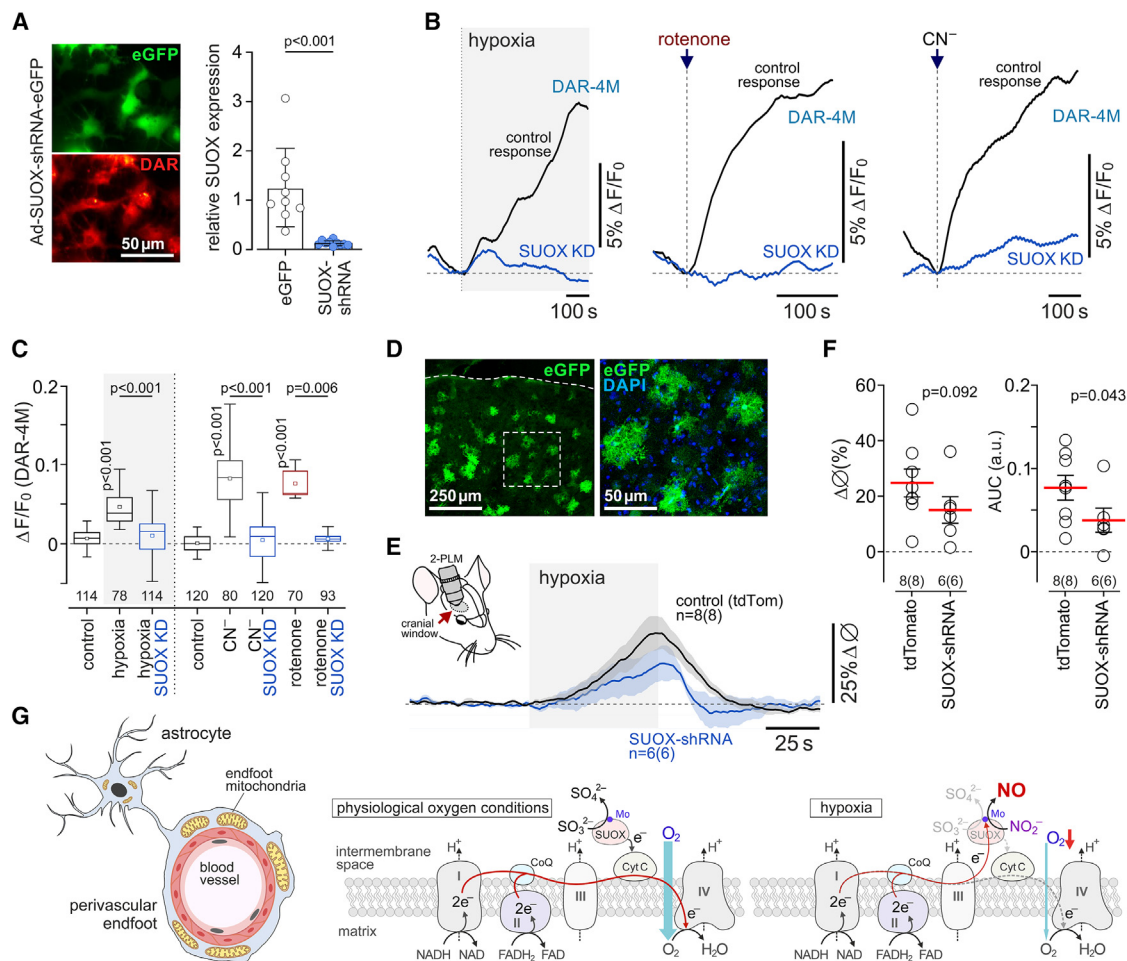


Figure 5. During hypoxia, NO is produced by the mitochondrial enzyme sulfite oxidase

(A) Astrocytes in culture transduced to express sulfite oxidase shRNA and loaded with DAR-4M. SUOX-shRNA reduced the expression of sulfite oxidase in astrocytes by 90%.

(B) Knockdown of sulfite oxidase (SUOX-KD) blocks NO production in astrocytes induced by hypoxia or mitochondrial inhibition with rotenone (2 μ M) or cyanide (100 μ M). Each trace illustrates averaged changes in DAR-4M fluorescence recorded in 7–20 individual astrocytes in separate experiments.

(C) Summary data illustrating peak changes in DAR-4M fluorescence in response to hypoxia or mitochondrial inhibition with rotenone or cyanide recorded in cortical astrocytes transduced to express EGFP or SUOX-shRNA (SUOX-KD). Numbers above the horizontal line indicate the numbers of individual astrocytes recorded in 4–8 separate cultures prepared from 3–6 animals. p values, ANOVA.

(D) Representative example of SUOX-shRNA expression in the cerebral cortex of an adult mouse that received an intracerebroventricular injection of AAV5-U6-SUOX-shRNA-EGFP vector at postnatal day 1.

(E) Hypoxia-induced cerebrovascular responses are reduced by SUOX-shRNA expression. Shown are changes in the diameter of penetrating cortical arterioles in response to 10% inspired O₂.

(F) Summary data illustrating peak and integral hypoxia-induced changes in cortical arteriole diameter in mice transduced to express tdTomato or SUOX-shRNA. The data are shown as individual values and means \pm SEM. n = number of vessels (number of animals). p values, unpaired t test.

(G) Schematic drawing of the mitochondrial ETC illustrating the proposed mechanism of NO production by astrocytes in response to hypoxia. In aerobic (physiological oxygen level) conditions, sulfite oxidase catalyzes the oxidation of sulfite to sulfate and transfers electrons to cytochrome c (CytC). During hypoxia, when mitochondrial respiration is inhibited and complex III and cytochrome c are fully reduced, sulfite oxidase transfers electrons and facilitates proton donation to reduce nitrite to NO. Mo, molybdenum.

involving measurements of hypoxia-induced changes in cerebral blood flow could be performed in awake animals. Finally, in this study, our main objective was to explore the cellular and physiological responses to acute hypoxia. The role of NO produced by sulfite oxidase in astrocyte mitochondria in the mechanisms underlying the responses and adaptation of the brain to chronic hypoxia remains to be investigated.

STAR★METHODS

Detailed methods are provided in the online version of this paper and include the following:

- KEY RESOURCES TABLE
- RESOURCE AVAILABILITY

- Lead contact
- Materials availability
- Data and code availability
- **EXPERIMENTAL MODEL AND STUDY PARTICIPANT DETAILS**
- **METHOD DETAILS**
 - Two-photon imaging *in vivo*
 - Processing of two-photon imaging data
 - Intracerebroventricular injections of viral vectors
 - Cell cultures and organotypic slice cultures
 - Optical recordings of NO production in astrocytes
 - Measurements of partial pressure of oxygen (PO₂)
 - Astrocyte sample preparation for nitrite measurements
 - Isolation and purification of astrocytes, RNA sequencing
 - Quantitative real-time PCR
 - Immunohistochemistry
- **QUANTIFICATION AND STATISTICAL ANALYSIS**

SUPPLEMENTAL INFORMATION

Supplemental information can be found online at <https://doi.org/10.1016/j.celrep.2023.113514>.

ACKNOWLEDGMENTS

This work was supported by The Wellcome Trust (Wellcome Senior Research Fellowship: ref. 200893; Wellcome Investigator Award: ref. 223057) and the British Heart Foundation (Ref. RG/19/5/34463).

AUTHOR CONTRIBUTIONS

A.V.G. conceived and directed the project; A.V.G., A.Y.A., P.R.A., A. Hobbs, and S.M.T. designed research; A. Braga, A. Hadjihambi, A.M., I.N.C., J.A.W., P.R.A., P.S.H., S.M.T., and S.N. performed research; A. Brazhe, A. Hadjihambi, A. Hobbs, A.S., A.V.G., A.Y.A., J.A.W., M.D., P.R.A., P.S.H., and S.M.T. analyzed data; S.M.T. generated key data supporting the involvement of sulfite oxidase; and A.V.G. wrote the paper. All authors revised the article critically for important intellectual content.

DECLARATION OF INTERESTS

The authors declare no competing interests.

Received: January 4, 2022

Revised: October 17, 2023

Accepted: November 14, 2023

Published: November 30, 2023

REFERENCES

1. Howarth, C., Gleeson, P., and Attwell, D. (2012). Updated energy budgets for neural computation in the neocortex and cerebellum. *J. Cereb. Blood Flow Metab.* 32, 1222–1232.
2. Buxton, R.B. (2010). Interpreting oxygenation-based neuroimaging signals: the importance and the challenge of understanding brain oxygen metabolism. *Front. Neuroenergetics* 2, 8.
3. Bailey, D.M. (2019). Oxygen, evolution and redox signalling in the human brain; quantum in the quotidian. *J. Physiol.* 597, 15–28.
4. Gourine, A.V., and Funk, G.D. (2017). On the existence of a central respiratory oxygen sensor. *J. Appl. Physiol.* 123, 1344–1349.
5. Willie, C.K., Tzeng, Y.C., Fisher, J.A., and Ainslie, P.N. (2014). Integrative regulation of human brain blood flow. *J. Physiol.* 592, 841–859.
6. Hoiland, R.L., Bain, A.R., Rieger, M.G., Bailey, D.M., and Ainslie, P.N. (2016). Hypoxemia, oxygen content, and the regulation of cerebral blood flow. *Am. J. Physiol. Regul. Integr. Comp. Physiol.* 310, R398–R413.
7. Devor, A., Sakadzic, S., Saisan, P.A., Yaseen, M.A., Roussakis, E., Srinivasan, V.J., Vinogradov, S.A., Rosen, B.R., Buxton, R.B., Dale, A.M., and Boas, D.A. (2011). "Overshoot" of O₂ is required to maintain baseline tissue oxygenation at locations distal to blood vessels. *J. Neurosci.* 31, 13676–13681.
8. Kasischke, K.A., Lambert, E.M., Panepento, B., Sun, A., Gelbard, H.A., Burgess, R.W., Foster, T.H., and Nedergaard, M. (2011). Two-photon NADH imaging exposes boundaries of oxygen diffusion in cortical vascular supply regions. *J. Cereb. Blood Flow Metab.* 31, 68–81.
9. Gjedde, A. (2002). Cerebral blood flow change in arterial hypoxemia is consistent with negligible oxygen tension in brain mitochondria. *Neuroimage* 17, 1876–1881.
10. Ndubuizu, O., and LaManna, J.C. (2007). Brain tissue oxygen concentration measurements. *Antioxid. Redox Signal.* 9, 1207–1219.
11. Gordon, G.R.J., Choi, H.B., Rungta, R.L., Ellis-Davies, G.C.R., and MacVicar, B.A. (2008). Brain metabolism dictates the polarity of astrocyte control over arterioles. *Nature* 456, 745–749.
12. Attwell, D., Buchan, A.M., Charpak, S., Lauritzen, M., MacVicar, B.A., and Newman, E.A. (2010). Glial and neuronal control of brain blood flow. *Nature* 468, 232–243.
13. Angelova, P.R., Kasymov, V., Christie, I., Sheikhbahaei, S., Turovsky, E., Marina, N., Korsak, A., Zwicker, J., Teschemacher, A.G., Ackland, G.L., et al. (2015). Functional oxygen sensitivity of astrocytes. *J. Neurosci.* 35, 10460–10473.
14. Hoiland, R.L., MacLeod, D.B., Stacey, B.S., Caldwell, H.G., Howe, C.A., Nowak-Flück, D., Carr, J.M., Tymko, M.M., Coombs, G.B., Patrician, A., et al. (2023). Hemoglobin and cerebral hypoxic vasodilation in humans: Evidence for nitric oxide-dependent and S-nitrosothiol mediated signal transduction. *J. Cereb. Blood Flow Metab.* 43, 1519–1531.
15. Ide, K., Worthley, M., Anderson, T., and Poulin, M.J. (2007). Effects of the nitric oxide synthase inhibitor L-NMMA on cerebrovascular and cardiovascular responses to hypoxia and hypercapnia in humans. *J. Physiol.* 584, 321–332.
16. Pelligrino, D.A., Wang, Q., Koenig, H.M., and Albrecht, R.F. (1995). Role of nitric oxide, adenosine, N-methyl-D-aspartate receptors, and neuronal activation in hypoxia-induced pial arteriolar dilation in rats. *Brain Res.* 704, 61–70.
17. Iwamoto, J., Yoshinaga, M., Yang, S.P., Krasney, E., and Krasney, J. (1992). Methylene blue inhibits hypoxic cerebral vasodilation in awake sheep. *J. Appl. Physiol.* 73, 2226–2232.
18. Bender, D., and Schwarz, G. (2018). Nitrite-dependent nitric oxide synthesis by molybdenum enzymes. *FEBS Lett.* 592, 2126–2139.
19. DeMartino, A.W., Kim-Shapiro, D.B., Patel, R.P., and Gladwin, M.T. (2019). Nitrite and nitrate chemical biology and signalling. *Br. J. Pharmacol.* 176, 228–245.
20. Kapil, V., Khambata, R.S., Jones, D.A., Rathod, K., Primus, C., Massimo, G., Fukuto, J.M., and Ahluwalia, A. (2020). The Noncanonical Pathway for In Vivo Nitric Oxide Generation: The Nitrate-Nitrite-Nitric Oxide Pathway. *Pharmacol. Rev.* 72, 692–766.
21. Lopez-Fabuel, I., Le Douce, J., Logan, A., James, A.M., Bonvento, G., Murphy, M.P., Almeida, A., and Bolaños, J.P. (2016). Complex I assembly into supercomplexes determines differential mitochondrial ROS production in neurons and astrocytes. *Proc. Natl. Acad. Sci. USA* 113, 13063–13068.
22. Kojima, H., Hirotani, M., Nakatsubo, N., Kikuchi, K., Urano, Y., Higuchi, T., Hirata, Y., and Nagano, T. (2001). Bioimaging of nitric oxide with fluorescent indicators based on the rhodamine chromophore. *Anal. Chem.* 73, 1967–1973.
23. Eroglu, E., Gottschalk, B., Charoensin, S., Blass, S., Bischof, H., Rost, R., Madreiter-Sokolowski, C.T., Pelzmann, B., Bernhart, E., Sattler, W., et al.

- (2016). Development of novel FP-based probes for live-cell imaging of nitric oxide dynamics. *Nat. Commun.* 7, 10623.
24. Ortega-Sáenz, P., Pardo, R., García-Fernández, M., and López-Barneo, J. (2003). Rotenone selectively occludes sensitivity to hypoxia in rat carotid body glomus cells. *J. Physiol.* 548, 789–800.
25. Arias-Mayenco, I., Gonzalez-Rodriguez, P., Torres-Torrelo, H., Gao, L., Fernandez-Aguera, M.C., Bonilla-Henao, V., Ortega-Saenz, P., and Lopez-Barneo, J. (2018). Acute O₂ Sensing: Role of Coenzyme QH(2)/Q Ratio and Mitochondrial ROS Compartmentalization. *Cell Metab.* 28, 145–158.e4.
26. Cahoy, J.D., Emery, B., Kaushal, A., Foo, L.C., Zamanian, J.L., Christopherson, K.S., Xing, Y., Lubischer, J.L., Krieg, P.A., Krupenko, S.A., et al. (2008). A transcriptome database for astrocytes, neurons, and oligodendrocytes: a new resource for understanding brain development and function. *J. Neurosci.* 28, 264–278.
27. Sparacino-Watkins, C.E., Tejero, J., Sun, B., Gauthier, M.C., Thomas, J., Ragireddy, V., Merchant, B.A., Wang, J., Azarov, I., Basu, P., and Gladwin, M.T. (2014). Nitrite reductase and nitric-oxide synthase activity of the mitochondrial molybdopterin enzymes mARC1 and mARC2. *J. Biol. Chem.* 289, 10345–10358.
28. Wang, J., Krizowski, S., Fischer-Schrader, K., Niks, D., Tejero, J., Sparacino-Watkins, C., Wang, L., Ragireddy, V., Frizzell, S., Kelley, E.E., et al. (2015). Sulfite Oxidase Catalyzes Single-Electron Transfer at Molybdenum Domain to Reduce Nitrite to Nitric Oxide. *Antioxid. Redox Signal.* 23, 283–294.
29. Hille, R., Hall, J., and Basu, P. (2014). The mononuclear molybdenum enzymes. *Chem. Rev.* 114, 3963–4038.
30. Klein, J.M., and Schwarz, G. (2012). Cofactor-dependent maturation of mammalian sulfite oxidase links two mitochondrial import pathways. *J. Cell Sci.* 125, 4876–4885.
31. Göbel, J., Engelhardt, E., Pelzer, P., Sakthivelu, V., Jahn, H.M., Jevtic, M., Folz-Donahue, K., Kukut, C., Schauss, A., Frese, C.K., et al. (2020). Mitochondria-Endoplasmic Reticulum Contacts in Reactive Astrocytes Promote Vascular Remodeling. *Cell Metab.* 31, 791–808.e8.
32. Khenouf, L., Gesslein, B., Brazhe, A., Oceau, J.C., Kutuzov, N., Khakh, B.S., and Lauritzen, M. (2018). Active role of capillary pericytes during stimulation-induced activity and spreading depolarization. *Brain* 141, 2032–2046.
33. Marina, N., Christie, I.N., Korsak, A., Doronin, M., Brazhe, A., Hosford, P.S., Wells, J.A., Sheikhbahaei, S., Humoud, I., Paton, J.F.R., et al. (2020). Astrocytes monitor cerebral perfusion and control systemic circulation to maintain brain blood flow. *Nat. Commun.* 11, 131.
34. Fordsmann, J.C., Murmu, R.P., Cai, C., Brazhe, A., Thomsen, K.J., Zambach, S.A., Lönstrup, M., Lind, B.L., and Lauritzen, M. (2019). Spontaneous astrocytic Ca²⁺ activity abounds in electrically suppressed ischemic penumbra of aged mice. *Glia* 67, 37–52.
35. Gourine, A.V., Kasymov, V., Marina, N., Tang, F., Figueiredo, M.F., Lane, S., Teschemacher, A.G., Spyer, K.M., Deisseroth, K., and Kasparov, S. (2010). Astrocytes control breathing through pH-dependent release of ATP. *Science* 329, 571–575.
36. Turovsky, E., Theparambil, S.M., Kasymov, V., Deitmer, J.W., Del Arroyo, A.G., Ackland, G.L., Comeaux, J.J., Allen, A.N., Huentelman, M.J., Kasparov, S., et al. (2016). Mechanisms of CO₂/H⁺ sensitivity of astrocytes. *J. Neurosci.* 36, 10750–10758.
37. Theparambil, S.M., Hosford, P.S., Ruminot, I., Kopach, O., Reynolds, J.R., Sandoval, P.Y., Rusakov, D.A., Barros, L.F., and Gourine, A.V. (2020). Astrocytes regulate brain extracellular pH via a neuronal activity-dependent bicarbonate shuttle. *Nat. Commun.* 11, 5073.
38. Turovsky, E.A., Braga, A., Yu, Y., Esteras, N., Korsak, A., Theparambil, S.M., Hadjihambi, A., Hosford, P.S., Teschemacher, A.G., Marina, N., et al. (2020). Mechanosensory signaling in astrocytes. *J. Neurosci.* 40, 9364–9371.
39. Bredt, D.S., Hwang, P.M., and Snyder, S.H. (1990). Localization of nitric oxide synthase indicating a neural role for nitric oxide. *Nature* 347, 768–770.
40. Hobbs, A.J., Fukuto, J.M., and Ignarro, L.J. (1994). Formation of free nitric oxide from L-arginine by nitric oxide synthase: direct enhancement of generation by superoxide dismutase. *Proc. Natl. Acad. Sci. USA* 91, 10992–10996.

STAR★METHODS

KEY RESOURCES TABLE

REAGENT or RESOURCE	SOURCE	IDENTIFIER
Antibodies		
Chicken anti-green fluorescent protein (GFP)	Abcam	Cat# AB13970, RRID: AB_2936447
Donkey anti-chicken Alexa Fluor 488	ThermoFisher	Cat# A78948, RRID: AB_2921070
Anti-GLAST (ACSA-1) phycoerythrin antibody	Miltenyi Biotec	Cat# 130-118-483, RRID: AB_2733722
Bacterial and virus strains		
AAV5-U6-SUOX-shRNA-eGFP	Vector Biolabs	Cat# shAAV-290554
AAV5-GFAP-tdTomato	Vector Builder	N/A
AAV5-CMV-geNOP	Next Generation Fluorescence Imaging	N/A
Ad-CMV-eGFP	Vector Builder	N/A
Ad-SUOX-shRNA-eGFP	Vector Biolabs	Cat# ADV-290554
Chemicals, peptides, and recombinant proteins		
Dextran, Texas Red™, 70,000 MW, Neutral	ThermoFisher	D1830
Fluorescein isothiocyanate–dextran	Sigma	FD40
Oregon Green™ 488 BAPTA-1, AM, cell permeant	Invitrogen	O6807
DAR-4M AM	Sigma	D9194
N(ω)-nitro-L-arginine methyl ester	Cayman Chemical	80210
Rotenone	Sigma	R8875
Myxothiazol	Sigma	T5580
KCN	Sigma	60178
FCCP	Sigma	C2920
Oligomycin	Sigma	04876
Tungstate	Sigma	223336
Sodium azide	Sigma	S2002
NaNO ₂	Sigma	237213
Anti-GLAST (ACSA-1) MicroBead Kit	Miltenyi Biotec	130-095-825
Experimental models: Cell lines		
Primary cortical astrocytes	N/A	N/A
Experimental models: Organisms/strains		
Sprague-Dawley rats	Charles River UK	N/A
C57BL/6J	Charles River UK	N/A
CD1 IGS	Charles River UK	N/A
Oligonucleotides		
qPCR primer Suox	ThermoFisher	Cat# Rn00579670_g1
Software and algorithms		
Andor iQ3 software	Andor	N/A
Spike2 7.12	Cambridge Electronics Design	https://ced.co.uk/products/spike2
Origin Pro	OriginLab	https://www.originlab.com/origin
FV10 ASW	Olympus	https://www.olympus-lifescience.com/en/
Deposited data		
Computer code for the analysis of imaging data		https://doi.org/10.5281/zenodo.10080722

RESOURCE AVAILABILITY

Lead contact

Further information and requests for resources and reagents should be directed to and will be fulfilled by the lead contact, Alexander V. Gourine (a.gourine@ucl.ac.uk).

Materials availability

This study did not generate new unique reagents.

Data and code availability

- Data reported in this paper will be shared by the [lead contact](#) upon reasonable request.
- The computer code used for the analyses of the *in vivo* imaging data is available via the link: <https://doi.org/10.5281/zenodo.10080722>.
- Any additional information required to reanalyze the data reported in this paper is available from the [lead contact](#) upon reasonable request.

EXPERIMENTAL MODEL AND STUDY PARTICIPANT DETAILS

All animal experiments were performed in accordance with the European Commission Directive 2010/63/EU (European Convention for the Protection of Vertebrate Animals used for Experimental and Other Scientific Purposes) and the UK Animals (Scientific Procedures) Act (1986) with project approval from the Institutional Animal Care and Use Committee of the University College London. The animals were group-housed and maintained on a 12-h light/dark cycle (lights on 07:00) and had *ad libitum* access to water and food.

Young Sprague-Dawley rats (100–150 g), adult C57BL/6J mice (2–3 months old), and adult CD1 IGS mice (2–3 months old) of both sexes were used to record hypoxia-induced cortical vascular responses and Ca^{2+} signals in cortical astrocytes. Primary cultures of cortical astrocytes and organotypic slices were prepared from the brains of both female and male rat pups (2- to 10-day post-gestation).

METHOD DETAILS

Two-photon imaging *in vivo*

Rats were anesthetized with isoflurane (2–4% in O_2 -enriched air). The femoral artery and vein were cannulated for recording of arterial blood pressure and administration of drugs, respectively. Isoflurane was discontinued after intravenous administration of urethane (1 g kg^{-1}) and α -chloralose (50 mg kg^{-1}). Adequate anesthesia was ensured by stability of arterial blood pressure and heart rate, and lack of cardiovascular responses to a paw pinch. The trachea was cannulated, and the animal was mechanically ventilated using a positive pressure ventilator (tidal volume: $\sim 1 \text{ mL}$ per 100 g of body weight; frequency: $\sim 60 \text{ strokes min}^{-1}$) with oxygen enriched air ($\sim 30\% \text{ O}_2$). During imaging, neuromuscular blockade was established using gallamine triethiodide (induction: 50 mg kg^{-1} , i.v.; maintenance: $10 \text{ mg kg}^{-1} \text{ h}^{-1}$, i.v.). Arterial PO_2 , PCO_2 , and pH were measured regularly and kept within physiological ranges by adjusting the tidal volume and the ventilator frequency. Body temperature was maintained at $37.0 \pm 0.5^\circ\text{C}$. Recordings of heart rate and arterial blood pressure were acquired and analyzed using Power1401 interface and Spike2 software (Cambridge Electronic Design).

Mice were anesthetized with a combination of fentanyl (0.05 mg kg^{-1} , i.v.), midazolam (5 mg kg^{-1} , i.v.) and medetomidine (0.5 mg kg^{-1} , i.v.). Room air supplemented with oxygen ($\sim 30\% \text{ O}_2$) was supplied through a nose mask, and mice breathed unaided throughout the experiment. Body temperature was maintained at $37.0 \pm 0.5^\circ\text{C}$.

The head of the animal was secured in a stereotaxic frame and a small circular craniotomy ($\sim 3 \text{ mm}^2$) was made in the parietal bone above the somatosensory cortex. Cortical cells were loaded with a Ca^{2+} -sensitive dye Oregon Green BAPTA 1 AM (OGB). OGB was first dissolved in DMSO and Pluronic F127 (20%). The solution containing OGB (1 mM) in artificial cerebrospinal fluid (aCSF; 124 mM NaCl, 3 mM KCl, 2 mM CaCl_2 , 26 mM NaHCO_3 , 1.25 mM NaH_2PO_4 , 1 mM MgSO_4 , 10 mM D-glucose saturated with 95% O_2 /5% CO_2 , pH 7.4) was delivered by microinjection via a glass micropipette at 2–4 sites within the targeted area of the cortex. The exposed surface of the brain was then covered with agarose (1%) and protected with a glass coverslip secured to the skull with a headplate and acrylic dental cement. Intravascular fluorescent dyes Texas Red (15 mg kg^{-1} ; MW 70,000, ThermoFisher) or Fluorescein isothiocyanate (FITC)-Dextran (15 mg kg^{-1} ; MW 40,000, Sigma) were administered intravenously.

Vascular and cellular responses in the cortex were recorded using an Olympus FV1000 microscope (Olympus), equipped with MaiTai HP DeepSee laser (Spectra-Physics). A 25 \times water-immersion objective (XLPlan N, NA 1.05; Olympus) was used. Fluorophores were excited in two-photon XYZ-t mode at 800 nm and images were acquired ~ 100 – $200 \mu\text{m}$ deep from the surface of the brain. Cortical arterioles (penetrating and intraparenchymal) were identified anatomically and by fluorescence of Texas Red or FITC-Dextran. Astrocytes were identified by their characteristic anatomical features such as endfeet. Laser power was kept to a minimum to reduce phototoxicity. Time-lapse recordings were made for up to 10 min with a period of hypoxia (10% or 15% O_2 in the inspired gas, balanced with N_2) lasting for $\sim 1 \text{ min}$. This protocol was selected in a series of pilot trials as it was found to evoke robust responses of brain parenchymal arterioles reaching peak dilations within this time period.

Processing of two-photon imaging data

Rigid-body shifts in the recorded data due to in-plane movements of the brain were corrected using the red fluorescence channel and an average over the first 20 frames as a template. The recorded imaging data were denoised by a two-step truncated singular value decomposition (SVD) projection algorithm. In short, each color channel video was split into overlapping spatial windows ("patches", 8x8 pixels), each window was then serialized to form a 2D matrix with single-pixel signals in rows; these matrices were approximated with truncated SVD. Temporal singular vectors were then collected in larger windows and approximated by a second truncated SVD. Inverse SVD transform provided denoised estimates of changes in fluorescence within each patch; estimates from overlapping patches were then averaged.

To measure changes in cortical vessel diameter, a line-scan was manually drawn across the widest part of the vessel and the lumen of the vessel was segmented using Chang-Vese active contours with constraints.^{32,33} Cell bodies of astrocytes were identified by an adaptive thresholding algorithm. Regions of interest (ROIs) corresponding to astrocyte cell bodies were manually selected for analysis. Changes in OGB fluorescence within each ROI were used for Ca^{2+} signal detection.^{33,34} An increase in OGB fluorescence was labeled as a Ca^{2+} transient if gaussian-smoothed (sigma = 1 frame) $\Delta F/F$ signal exceeded a threshold of 2.5 standard deviations (obtained via median absolute deviation robust estimator) for at least 3 consecutive frames.

Astrocyte endfeet were identified as OGB-stained structures encircling penetrating arterioles. To analyze Ca^{2+} responses in the endfeet, a special algorithm was applied to trace the deformations of the endfeet associated with changes in vessel diameter. In each frame, the circumference of an endfoot around a vessel was tracked and resampled along the resulting closed path to a constant number of steps (360), corresponding to rotation degree ϕ in polar coordinates with the origin at the center of the vessel. First, a ridge-enhancing filter was applied to each frame in a crop around a vessel of interest in the green fluorescence channel. These ridge-enhanced frames were resampled to polar coordinates with the origin at the vessel center, and the endfoot was segmented as a brightness-weighted path from $\phi = 0$ to $\phi = 360$ within the graph of connected local maxima locations with constraint on matching radius coordinates for the start and the end of the path and path length. OGB fluorescence signals were then sampled along the circumference of the endfeet in 360 ϕ providing 1 vector column of OGB fluorescence per each frame, resulting in a 2D representation of Ca^{2+} changes, with time on the X axis and the rotation angle of the circumference on the Y axis. This kymograph of changes in OGB fluorescence was used for the detection of Ca^{2+} signals in the endfeet. Increases in OGB fluorescence above 5% $\Delta F/F$ and larger than 64 pixels (frames \times degrees) were labeled as Ca^{2+} signals in the endfeet. Maximal projections of changes in $\Delta F/F$ signals along the Y axis were used to plot Ca^{2+} signal traces.

Intracerebroventricular injections of viral vectors

In a series of validation trials conducted in rats and mice the expression of SUOX-shRNA induced by AAV5-U6-SUOX-shRNA-eGFP vector in the rat brain was found to be very limited. Therefore, mice were used in the experiments involving targeting of cortical astrocytes to express SUOX-shRNA. The viral vectors were administered to 1-day post-gestation (P1) neonatal CD1 IGS mice via unilateral intracerebroventricular injection (AP: -1.5mm ; ML: 0.5mm ; DV: 1.3mm). The pups were anesthetized with isoflurane and injected with viral vector AAV5-U6-SUOX-shRNA-eGFP (10^{11} viral genomes; Vector Biolabs) or AAV5-GFAP-tdTomato (control; 10^8 viral genomes, Vector Builder) using a 33-gauge needle (injection volume $<1.5\ \mu\text{L}$). After the injections, the pups were returned to the dam and were used in experiments at 7–8 weeks of age.

Cell cultures and organotypic slice cultures

Primary cultures of cortical astrocytes were prepared from the brains of rat pups (P2–3 of either sex).^{35–38} The animals were euthanized by exposure to isoflurane, the brains were removed, and the cortical regions were separated by dissection. After isolation, the cells were plated on poly-D-lysine-coated coverslips and maintained at 37°C in a humidified atmosphere of 5% CO_2 and 95% air for a minimum of 10 days before experiments. Viral vectors to express the genetically encoded NO sensor geNOp (AAV5-CMV-geNOp, titer 1.3×10^{11} ; Next Generation Fluorescence Imaging), enhanced green fluorescent protein (Ad-CMV-eGFP, titer 1.0×10^{10} ; Vector Builder), or SUOX-shRNA-eGFP (Ad-SUOX-shRNA-eGFP, titer 1.5×10^{10} ; Vector Biolabs) were added to the incubation medium after 5–7 days from the time of cell culture preparation.

Neuronal cultures were prepared from the cerebellum as the expression of neuronal NOS is highest in this part of the brain.³⁹ Rat pups (P6–8 of either sex) were euthanized by isoflurane, the brains were removed, and the cerebella were separated in ice-cold Hank's Balanced Salt Solution (HBSS) buffer. Cells were dissociated after tissue incubation with TrypLE enzyme (ThermoFisher; 15 min at 37°C) and suspended in Neurobasal medium containing B-27 supplement, 2 mM L-Glutamine, 25 mM K^+ , $100\ \text{U mL}^{-1}$ penicillin, and $0.1\ \text{mg mL}^{-1}$ streptomycin. Cells were then plated on poly-D-lysine-coated coverslips and maintained at 37°C in a humidified atmosphere of 5% CO_2 and 95% air for a minimum of 5 days before experiments.

Organotypic cortical slices were prepared from the brains of rat pups (P8–10 of either sex).¹³ The animals were euthanized by isoflurane, the brains were removed and placed in ice-cold HBSS without Ca^{2+} , with added 20 mM glucose (total 25.6 mM), 10 mM MgCl_2 , 1 mM HEPES, 1 mM kynurenic acid, 0.005% phenol red, $100\ \text{U mL}^{-1}$ penicillin, and $0.1\ \text{mg mL}^{-1}$ streptomycin. A sequence of coronal slices ($400\ \mu\text{m}$) was cut at the level of the somatosensory cortex and plated on Millicell-CM organotypic culture membrane inserts (Merck Millipore). Slices were cultured in a medium containing 50% Optimem-1, 25% fetal bovine serum (FBS), 21.5% HBSS; 25 mM glucose, $100\ \text{U mL}^{-1}$ penicillin, and $0.1\ \text{mg mL}^{-1}$ streptomycin. After 3 days, the plating medium was removed and replaced with Dulbecco's Modified Eagle medium containing 10% FBS, 2 mM L-Glutamine, $100\ \text{U mL}^{-1}$ penicillin, and $0.1\ \text{mg mL}^{-1}$

streptomycin. The medium was subsequently replaced twice a week. The slices were used in the experiments after 7–10 days of incubation.

Optical recordings of NO production in astrocytes

Optical recordings of NO production in cultured astrocytes were performed using an inverted epifluorescence Olympus microscope, equipped with a cooled CCD camera (Clara model; Andor). The cells were loaded with the NO sensitive fluorescent probe DAR-4M AM (Sigma; 10 μ M, 30 min incubation at room temperature) or transduced to express the genetically encoded NO sensor geNOp. Recordings were performed in a custom-made flow-through imaging chamber at $\sim 32^{\circ}\text{C}$ in aCSF saturated with 95% O_2 /5% CO_2 (pH 7.4). The rate of chamber perfusion with aCSF was 4 mL min^{-1} . DAR-4M fluorescence was excited by using a Xenon arc lamp and an Optoscan Monochromator (Cairn Research) at 560/10 and the fluorescence emission was recorded at 590 nm; geNOp fluorescence was excited at 488/10 nm and the fluorescence emission was recorded at 535 nm.

Hypoxic conditions *in vitro* were induced by the displacement of oxygen in the medium by argon. In all experiments in cell cultures and organotypic slices the hypoxic challenge was applied for 5–15 min. A representative profile of PO_2 changes in the recording chamber during argon displacement is illustrated by Figure 2F. All test drugs were applied ~ 10 min before the hypoxic challenge. Imaging data were collected and analyzed using Andor iQ3 software (Andor).

Measurements of partial pressure of oxygen (PO_2)

In the experiments in organotypic slices, PO_2 was recorded using optical fluorescence probes (250 μm tip diameter, OxyLite system, Oxford Optronix) placed on the surface of the slice.¹³

Astrocyte sample preparation for nitrite measurements

Accumulation of NO_2^- in astrocytes and astrocyte mitochondria was determined by chemiluminescence assay.⁴⁰ After 12 days in culture, astrocytes were washed with phosphate-buffered saline (PBS) and incubated for 60 min in HBSS containing NO_2^- (NaNO_2) at concentration of 0, 5, 10, 30 or 100 μM . Samples were then washed with PBS (3x), treated with trypsin (5 min), and centrifuged (at 240 \times g, 5 min). The supernatant was removed, and the cell pellets were resuspended in PBS to washout the extracellular NO_2^- . This procedure was repeated twice. After the last wash, the cells were resuspended in 10 mL ddH_2O to induce osmotic lysis and the samples were flash-frozen and stored at -80°C until assayed. In a separate set of the experiments, pure astroglial cultures were incubated for 60 min with NO_2^- (0, 5, 10, 30 or 100 μM). After harvesting by trypsinization, the cells were washed twice in PBS and incubated on ice for 15 min. Mitochondria were isolated by a series of centrifugations at 600 \times g, 900 \times g and 12,000 \times g. The mitochondrial pellet was then resuspended in ddH_2O to induce osmotic lysis of the organelles; the samples were frozen and stored at -80°C until assayed.

Isolation and purification of astrocytes, RNA sequencing

Young adult male rats (~ 100 g) and rat pups (P3 of either sex) were used to isolate cortical astrocytes.³⁶ The animals were euthanized by isoflurane inhalation overdose and the brains were isolated. The cortex was dissected and the meninges were removed. The tissue was enzymatically dissociated to make a suspension of individual cells. The samples were passed through a 45 μm Nitex mesh to remove undissociated cell clumps and after addition of myelin removal beads (Miltenyi Biotec), passed through a MACS column (Miltenyi Biotec). The second (positive) magnetic separation was then performed using astrocyte-specific anti-GLAST (ACSA-1) antibodies conjugated to the magnetic beads (Miltenyi Biotec). Cell purity was assessed by using anti-GLAST (ACSA-1) phycoerythrin antibody (Miltenyi Biotec) and flow cytometry (CyanADP Cytometer, Beckman Coulter). FACS analysis confirmed >95% purity of isolated astrocytes. Purified cells were harvested by centrifugation at 2000 \times g for 5 min. The cell pellet was then used for RNA extraction. Separately, cultured astrocytes were individually collected using patch pipettes (tip ~ 5 μm) made of borosilicate glass. One biological replicate consisted of 20–25 pooled cells from 3 to 4 cultures.

Total RNA was isolated using RNeasy Plus Micro Kit (Qiagen) following the manufacturer's protocol and RNA quality was assessed using the RNA 6000 Pico Kit on a 2100 Bioanalyzer (Agilent Technologies). RNA sequencing, read mapping, and expression level estimation were performed as described.³⁶ Reads were aligned to the rat reference genome RGSC3.4.64 with TopHat 1.3.3. Cufflinks v1.0.2 was used to assemble and quantify the transcriptome of each sample. A union set of transcripts in all samples was generated with Cuffcompare, and differential expression was assessed with Cuffdiff. Expression level is reported as fragments per kilobase of transcript sequence per million mapped fragments (FPKM) values.

Expression of genes encoding nitric oxide synthases and all known metalloproteins with nitrite reductase activity^{18,19} were compared across the three conditions: cultured cortical astrocytes (1), and cortical astrocytes acutely isolated from neonatal (2) and young adult (2) rats. Genes included in the analysis were as follows: *Aox4*, aldehyde oxidase 4; *Cygb*; cytoglobin, *Mtarc1*; mitochondrial amidoxime reducing component 1, *Mb*; myoglobin, *Mocs3*; molybdenum cofactor sulfuryase, *Mocs2*; molybdenum cofactor synthesis 2, *Mocs3*; molybdenum cofactor synthesis 3, *Ngb*; neuroglobin, *Nos1*; nitric oxide synthase neuronal, *Nos2*; nitric oxide synthase inducible, *Nos3*; nitric oxide synthase endothelial, *Suox*; sulfite oxidase, *Xdh*; xanthine dehydrogenase/oxidase. Plots were created using the ggplot2 package in R.

Quantitative real-time PCR

Quantitative real-time PCR (RT-qPCR) was used to determine the level of sulfite oxidase mRNA expression in cortical astrocytes transduced to express eGFP ($n = 9$) or SUOX-shRNA-eGFP ($n = 10$). Total RNA was extracted, purified (RNeasy micro kit, 74004, Qiagen), and reverse transcribed using the QuantiTect Reverse Transcription Kit (205311, Qiagen). PCR reactions were performed in 20 μ L volumes using the TaqMan Universal Master Mix II (4440040, ThermoFisher) with the final volume of 9 μ L cDNA, equivalent to 24 ng RNA sample template per reaction. PCR reactions were performed in duplicates using the TaqMan assay (Suox, Rn00579670_g1, 81 bp amplicon length, ThermoFisher) as detection method, and an Agilent Technologies Aria Mx RT-PCR system (Agilent). Relative *Suox* expression values were calculated using the comparative CT method ($\Delta\Delta C_t$) and presented as arbitrary units of expression, normalized to the expression of the Ubiquitin C gene (Rn01789812_g1, 88 bp amplicon length, ThermoFisher).

Immunohistochemistry

Mice were terminally anesthetized with isoflurane and transcardially perfused with saline, followed by ice-cold 4% paraformaldehyde solution. The brains were removed, fixed overnight in 4% paraformaldehyde, and sectioned serially using a cryostat. Brain sections (30 μ m) were incubated overnight at room temperature with chicken anti-GFP antibodies (1:500 dilution; Abcam), followed by incubation with fluorochrome-conjugated donkey anti-chicken Alexa Fluor 488 secondary antibodies (1:1,000 dilution; ThermoFisher) for 2 h. Sections were mounted using Fluoroshield antifade mounting medium. Fluorescent images were acquired using a confocal microscope (Leica SP8) with a 25 \times objective.

QUANTIFICATION AND STATISTICAL ANALYSIS

Data were compared by linear mixed-effects model test for nested data with random intercepts, Kruskal-Wallis ANOVA, one way ANOVA with Tukey post-hoc test, or t test as appropriate. Linear mixed-effects models were used to analyze the effects of treatments on vascular responses and Ca^{2+} signals in astrocyte cell bodies and endfeet; the presence or absence of the drug was treated as a fixed effect, and intercepts for each animal and structure of interest were treated as random effects. p values were determined by post-estimation inference using Wald tests. Linear mixed-effect model analysis was performed in the "statsmodels" library for Python. The other statistical tests were performed using OriginPro software. The data are shown as individual values and means \pm SEM or box-and-whisker plots. Details of the statistical tests applied are provided within the figure legends. Differences with a p value of less than 0.05 were considered to be significant.